ARTICLE

JOURNAL`S UNIVERSITY OF BABYLON FOR ENGINEERING SCIENCES (JUBES)

مـــجلـة جـــامعة بـــابـل للعلـــوم الهندسية

Vol. 34, No. 1. \ 2026 ISSN: 2616 - 9916

Numerical Investigation of a Square Finned Heat Sink at Different Angles of Inclination

Fatima R. Nada[1] Khudheyer S. Mushatet[1]

[1] Department of Mechanical Engineering, Faculty of Engineering, University of Thi-Qar, 64001, Iraq

fatima.r.n@utq.edu.iq

Received:	24/12/2025	Accepted:	1/2/2026	Published:	31/3/2026

Abstract

This study presents a numerical investigation of a finned heat sink in forced convection flow. Tests were conducted on a square fin with varying angles of inclination, heights, and distances between fins. These parameters were examined at different Reynolds numbers within the turbulent range (from 5000 to 25000) and a heat flux of 5000 W/m². The heat distribution and flow behavior around the heat sink were modeled using the full Navier-Stokes and energy equations. The simulations were performed using ANSYS Fluent with the k-ε model. Results indicated that decreasing fin spacing from 6mm to 2mm led to 9% reduction in surface temperature and an increase in the Nusselt number by 41%, highlighting a significant enhancement in convective heat transfer. Similarly, variations in fin height showed a noticeable influence on thermal behavior, resulting by 16% reduction in surface temperature and enhancing the Nusselt number by 94%, and an inclination of 15 was found to provide the optimal thermal performance among the investigated angles, achieving the lowest surface temperature by 6% .

Keywords: Heat Sink, Square fins, Thermal performance.

1. Introduction

Effective heat dissipation greatly affects the thermal performance and dependability of modern electrical devices and energy systems, as heat generation is steadily rising due to the power density of components. Enhancemed thermal dissipation technique has become a significant engineering issue [1]. The heat sink with expanded surfaces is one of several thermal improvement techniques that are employed due to their simplicity, high surface area, and cost-effectiveness. Many investigations have focused on the thermal behavior of heat sinks by improving geometric designs [2]. Extensive research was conducted to enhance the thermal behavior of a fin heat sink through geometric optimization. Huang et al.[3] studied the development of heat sinks that are utilized for cooling high-power LEDs, where high temperature negatively affects energy efficiency, brightness, and lifespan of LEDs. ANSYS Fluent 15 was used to simulate the system under a temperature of 25 ˚C, atmospheric pressure, and input power of 4 watts. Jaffel [4] emphasized the thermal behavior of heat sinks, including different fin models like the flat plate, the perforated, the perforated cross-cut, the cross-cut, the serpentine, and the zigzag fins. Fluent 15 with k-ε turbulence model, Navier-Stokes, and energy equations were used to simulate and analyze the heat transfer by forced convection in the fins. The Reynolds number was (23597 to 3848.9) and the associated heat flux (3954 to38357W/m²). The results displayed that the perforated-cut fins exhibit high heat transfer and best thermal

performance; both the heat transfer coefficient (h) and the Nusselt number (Nu) increased with the Reynolds number (Re). Mushatet and Bader[5] used parallel ribs with varying angles of attack, oriented perpendicular to the primary flow direction. The primary objective of the study was to identify the rib angle that maximizes heat transfer and improves the overall thermal performance within the heated duct. The rib height-to-duct height ratio (e/H) was maintained at 0.6 throughout the study. The P/E ratio was 10. For inclined ribs, the angles of attack (α) were altered from 30° to 90° and evaluated at a constant mass flow rate (MFR) of 0.022 kg/s. Sivasankaran et al.[6] studied the comparison of the thermal behavior for two models of aluminum heat sinks (parallel plate and crosscut fins).The distance between the fan and heat sink was varied (0 to 60 mm). The heat input ranged from 20W to 60W. Jabber et al.[7] studied five different lengths of heat sink made of three materials (steel, copper, and aluminum) for a single square-type heat sink, which was previously used in high-performance graphic cards with built-in motherboards, to assess its thermal conductivity and heat dissipation capability at nearly 60˚C operating temperature. Chin et al.[8] focused on the improvement of heat transfer under forced convection using staggered perforated fin arrays. The internal height and width of the channel are 50 and100 mm, respectively. The channel is constructed with a transparent 5 mm acrylic sheet with a thermal conductivity of 0.17 Wm-1 K-1 to minimize heat loss. Air is supplied by a blower (ebmpapst, Germany) with controllable flow velocity (maximum 12 ms-1). Mushatet et al.[9] carried out a numerical study to examine the flow and heat transfer characteristics in a sudden expansion channel equipped with rectangular adiabatic obstacles positioned on both the upper and lower walls downstream of the expansion. Different values of Reynolds number (Re = 50, 100, 150, and 200) were selected while the value of Prandtl number was equal to 0.7. Sukumar et al.[10] demonstrated the design of the rectangular heat sink that includes continuous, interrupted, and other designs with holes. The heat sinks were designed by PRO-E Wildfire 5, and analysis was performed using CFD with ANSYS Fluent. Annuar and Ismai [11] studied and analyzed the heat transfer of a heat sink. The fins were arranged in various ways, including (inline, staggered, and random), the COSMOL Multiphysics and inlet Atum A450 CPU used in this study for testing, with airflow conditions simulation and power dissipation. Their results showed that the random fin arrangement displayed better thermal performance. Hussein et al.[12] Investigated the effectiveness of perforated fins subject to forced convection, he designed circular perforations along the length of the fins. The number of perforations was between 24 and 56. Three setups of aluminum fins were tested: flat edge fins, rectangular edge fins, and rectangular edge fins with circular perforations. They tested four voltage levels (37.5, 50, 62.5, and 75V). Nashee and Mushatet[13] presented an analysis of turbulent airflow in rectangular channels equipped with ribs. The simulations were performed using ANSYS Fluent 17. The tested channel has Length (L), Height (H), Width (W), and Thickness (1000 mm,60 mm,150 mm, and2 mm). The used rib lengths are 150 mm ,60 mm, and 30 mm. Experiments are conducted at the Reynolds numbers ranging from 10,000 to 35,000. Al Kindi [14] studied the heat sink in a duct; a 3D computational model was used, and ANSYS Fluent for numerical solution. Experimental tests were collected with WL-352 Gunt. Tariq et al. [15] studied the impact of combining side slots in plate and longitudinal perforations in fin heat sinks to improve thermal performance and decrease pressure losses. Two novel models, including NPFHS-1 (with square perforations) and NPFHS-2 (with circular perforations), were used, with a Reynolds number range of 13.049 to 52.195. Abdelmohimen et al. [16] examined the effect of inserting

rods across the fins of the heat sinks to improve their thermal efficiency. A simulated solution with shear stress transport (SST) kω model, four configurations including 2, 4, 6 pairs, and a baseline with no rod under two air flow directions (jet and inward flow) were used. Mohammed and Razuqi[17] focused on investigating the heat transfer performance of a copper heat sink equipped with aligned rectangular fins subjected to forced air flow, with a thermal conductivity of 401 W/m·K, equipped with 72 rectangular fins. The Reynolds number was varied between 4000 and 16000, with a constant heat flux ranging from 10000 to 70000 W/m². Sertkaya et al.[18] studied the heat transfer of a heat sink that includes 64 fins organized in a straight inline construction on a base plate measuring 0.12×0.12 meters under laminar natural convection conditions. Two designs of circular pin fins were used, each with two different heights of 30 and 40 mm. The input heating power varied from 5W to over 50W. Gurav et al.[19] investigated the thermal distribution and fluid flow of a pin fin heat sink (PFHS) with forced convection conditions, with inclined or linear wing, the velocities were form 1m/s to 2m/s and base temperature ranging from 333k to 353k. Al-Luhaibi and Nazzal [20] investigated the thermal behavior improvement of rectangular heat sinks with perforated fins. Two patterns were used: horizontally variable perforations (PHS-HV), where hole diameters increase horizontally, and vertically variable perforations (PHS-VV), where hole diameters increase vertically. Mushatet and Fayyad [21] investigated the absorber plate that was artificially roughened using rectangular ribs of varying heights(1, 2, and 3 cm). The air mass flow rate ranged from 0.01559 to 0.042 kg/s. The channel was a rectangular cross-section with dimensions (1250mm x 360mm x 50mm) (L x H x W), The absorber plate was roughened with rectangular ribs with a dimension of 36 cm long, 2cm wide, and the height ranging from 1 cm to 3cm. Çiçek [22] executed a numerical study to analyze the thermal performance of phase change material (PCM) and base heat sinks (HPCM) for electronic cooling application three types of PCMs-RT-28HC, RT-31, and RT-54HC were analyzed based on their diverse thermophysical properties under different heat fluxes (3.6, 4.2, and 4.8kW/m²). Nashee and Mushatet [23] Both experimental and numerical investigations were conducted to evaluate the heat transfer enhancement and overall thermal performance of a rectangular air turbulator. Sukri and Wanatasanappan [24] evaluated the thermal performance of different heat sink configurations (rectangular plate fins, rectangular pin fins, and separated short plate fins), the base plate thickness (2.5 mm and 5mm), and heat sink material (copper and aluminum) with three thermal loads: 60W, 70W, and 80W. The results showed that the rectangular plate at the fin heat sink showed higher thermal performance compared to other designs. Azirul et al. [25] studied the enhancement of photovoltaic–thermoelectric (PVTE) systems' performance by optimizing heat sink designs and fluid flow parameters. They solved the issue of overheating in photovoltaic (PV) panels' temperatures. Nazeel et al. [26] investigated the impact of various alloy materials on thermal performance, including pure aluminum, aluminum-beryllium alloy, and aluminum-copper.

Nomenclature

Ac Across-sectional area

D_h Hydraulic diameter (m)

H Height of fins

h Coefficient of convective heat transfer (W/m². K)

k Thermal conductivity (W/m. K)

L Length of heat sink (m)

Nu Nusselt number

P The perimeter

q Heat flux per area (w/m)

Re Reynolds number

Tw Heated wall temperature (˚c)

Tb Bulk temperature (˚c)

t Thickness of heat sink (m)

d Distance between fins (m)

W Width of heat sink (m)

Greek letters

μ Dynamic viscosity (Kg/s.m³)

ρ Density(kg/m³)

ffeΓ Effective thermal diffusivity (m² /s)

2. Physical model

The geometry consists of a three-dimensional aluminum heat sink mounted at the center of a rectangular channel. The channel dimensions are 60mm in height, 80mm in width, and 1000mm in length. The heat sink has a square base of 60×60mm and a base thickness of 2mm. It consists of 36 square fins arranged in a uniform 6×6 array across the base, as shown in Fig. 1. In this section, several cases are considered to investigate the influence of geometric parameters. The first case considers three spacings between fins (2, 2, and 6mm). The second case corresponds to three fin heights (20, 27, and 35 mm) with a spacing of 2 mm, and the third case involves three installation angles of fins (5˚, 15˚, and 25˚).

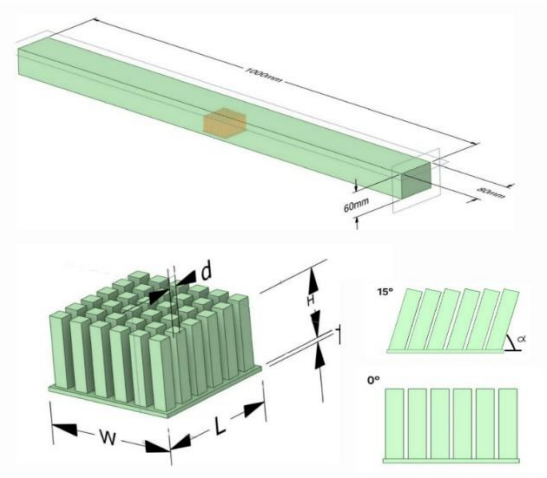

Fig.1: Illustrative diagram of the heat sink inside the rectangular channel.

3. Mathematical and numerical analysis

The description of the airflow inside the rectangular channel with the mounted heat sink under turbulent conditions is carried out by solving the time-averaged governing equations of mass (continuity, momentum, and energy [27]), with turbulence modeled using the k-ε approach.

$$\frac{\partial u}{\partial x}+\frac{\partial u}{\partial y}+\frac{\partial w}{\partial z}=0 \quad (1)$$

$$\rho\left(\frac{\partial u^2}{\partial x^2}+\frac{\partial uv}{\partial y}+\frac{\partial uw}{\partial^z}\right)= -\frac{\partial P}{\partial x}+\frac{\partial}{\partial x}\left(2\mu eff\frac{\partial u}{\partial x}\right)+\frac{\partial}{\partial y}\left(\mu eff\frac{\partial u}{\partial y}\right)+ \frac{\partial}{\partial z}\left(\mu eff\frac{\partial u}{\partial z}\right)+\frac{\partial}{\partial y}\left(\mu eff\frac{\partial v}{\partial x}\right)\frac{\partial}{\partial z}\left(\mu eff\frac{\partial w}{\partial x}\right) \quad (2)$$

$$\rho\left(\frac{\partial vu}{\partial x}+\frac{\partial v^2}{\partial y}+\frac{\partial vw}{\partial^z}\right)= -\frac{\partial P}{\partial y}+\frac{\partial}{\partial x}\left(\mu eff\frac{\partial v}{\partial x}\right)+\frac{\partial}{\partial y}\left(2\mu eff\frac{\partial v}{\partial y}\right)+\frac{\partial}{\partial z}\left(\mu eff\frac{\partial v}{\partial z}\right)+\frac{\partial}{\partial x}\left(\mu eff\frac{\partial u}{\partial y}\right)+ \frac{\partial}{\partial z}\left(\mu eff\frac{\partial w}{\partial y}\right) \quad (3)$$

$$\rho\left(\frac{\partial wu}{\partial x^2}+\frac{\partial wv}{\partial y}+\frac{\partial w^2}{\partial^z}\right)= -\frac{\partial P}{\partial z}+\frac{\partial}{\partial x}\left(\mu eff\frac{\partial w}{\partial x}\right)+\frac{\partial}{\partial y}\left(\mu eff\frac{\partial w}{\partial y}\right)+ \frac{\partial}{\partial z}\left(2\mu eff\frac{\partial w}{\partial z}\right)+\frac{\partial}{\partial x}\left(\mu eff\frac{\partial u}{\partial z}\right)+\frac{\partial}{\partial y}\left(\mu eff\frac{\partial v}{\partial z}\right) \quad (4)$$

$$\frac{\partial uT}{\partial x}+\frac{\partial vT}{\partial y}+\frac{\partial wT}{\partial z}=$$
$$\frac{\partial}{\partial x}\left(\Gamma_{eff}\frac{\partial T}{\partial x}\right)+\frac{\partial}{\partial y}\left(\Gamma_{eff}\frac{\partial T}{\partial y}\right)+$$
$$\frac{\partial}{\partial z}\left(\Gamma_{eff}\frac{\partial T}{\partial z}\right) \quad (5)$$

3.1 The standard k-ε model

The k–ε model represents turbulence using two variables: k, the turbulent kinetic energy, and ε, its rate of dissipation. This approach approximates the effects of turbulence on momentum and heat transfer.

$$\rho\left(\frac{\partial}{\partial x}(ku)+\frac{\partial}{\partial y}(kv)+\frac{\partial}{\partial z}(kw)\right)=$$
$$\frac{\partial}{\partial x}\left(\frac{\mu_t}{\sigma_k}\frac{\partial k}{\partial x}\right)+\frac{\partial}{\partial y}\left(\frac{\mu_t}{\sigma_k}\frac{\partial k}{\partial y}\right)+\frac{\partial}{\partial z}\left(\frac{\mu_t}{\sigma_k}\frac{\partial k}{\partial z}\right)+G-$$
$$\rho\varepsilon \quad (6)$$

For energy dissipation rate (ε)[28]:

$$\rho\left(\frac{\partial}{\partial x}(\varepsilon u)+\frac{\partial}{\partial y}(\varepsilon v)+\frac{\partial}{\partial z}(\varepsilon w)\right)=\frac{\partial}{\partial x}\left(\frac{\mu_t}{\sigma_\varepsilon}\frac{\partial \varepsilon}{\partial x}\right)+\frac{\partial}{\partial y}\left(\frac{\mu_t}{\sigma_\varepsilon}\frac{\partial \varepsilon}{\partial y}\right)+\frac{\partial}{\partial z}\left(\frac{\mu_t}{\sigma_\varepsilon}\frac{\partial \varepsilon}{\partial z}\right)+C_{1\varepsilon}\rho\frac{\varepsilon}{k}G-$$
$$C_{2\varepsilon}\rho\frac{\varepsilon^2}{k} \quad (7)$$

Where G is referred to as the generation term

$$G=$$
$$\mu_t\left[2\left(\frac{\partial u}{\partial x}\right)^2+2\left(\frac{\partial v}{\partial y}\right)^2+2\left(\frac{\partial w}{\partial z}\right)^2+\left(\frac{\partial v}{\partial y}\frac{\partial u}{\partial x}\right)^2+\left(\frac{\partial v}{\partial z}\frac{\partial w}{\partial x}\right)^2+\right.$$
$$\left.\left(\frac{\partial v}{\partial z}\frac{\partial w}{\partial y}\right)^2\right] \quad (8)$$

Also, k,

$$k=\frac{1}{2}\left(\overline{u'^2}+\overline{v'^2}+\overline{w'^2}\right) \quad (9)$$

$$\varepsilon=\overline{e'_{ij}\acute{e}_{ij}} \quad (10)$$

The dissipation rate (ε) and turbulent kinetic energy (k) are selected as two properties to resolve the turbulent viscosity (μ_t). Where

$$\mu_t=\rho c_\mu\frac{k^2}{\varepsilon} \quad (11)$$

3.2 Hydrodynamic parameters

Inlet Reynolds number was calculated as:

$$Re = \frac{\rho_{\cup aV}\, Dh}{\mu} \tag{12}$$

$$D_h = \frac{4Ac}{P} = \frac{4bh}{2(b+h)} = \frac{2bh}{b+h} \tag{13}$$

The average coefficient of convective heat transfer h will be calculated as [29]

$$h = \frac{q}{T_w{}^{-}T_b} \tag{14}$$

The Nusselt number will be calculated

$$N_u = \frac{hD_h}{k} \tag{15}$$

3.3 Boundary conditions

A numerical simulation was conducted for a heat sink placed within a rectangular channel. The applied boundary conditions were defined as:

Notes	value
Inlet velocity	1.4-7.01m/s
Constant inlet temperature	298 K
Applied heat flux	5000 W/m²
All walls	No- slip
Pressure outlet	0 pa gauge

3.4 Numerical methodology

The finite volume technique with a staggered grid arrangement was employed to discretize the governing model equation on the considered computational domain. ANSYS Fluent 21 was used to obtain the current results.

The dimensions of the channel and the heat sink were selected within the range reported in previous studies [30] [31], ensuring realistic design and adequate flow development along the channel.

3.5 Mesh generation

Discretization of the spatial domain requires that the flow field be divided into small control volumes. Various types of control volumes can be employed, including hexahedral and tetrahedral elements, as well as structured or unstructured meshes. In the present study, a tetrahedral mesh was adopted, as illustrated in Fig.2, due to its suitability for simulating

separated flow. The mesh was refined in regions near the walls and fins, where turbulators are present. The Tw was employed to carry out the grid independence test at Re=10000. Table 1 summarizes the grid results for cases.

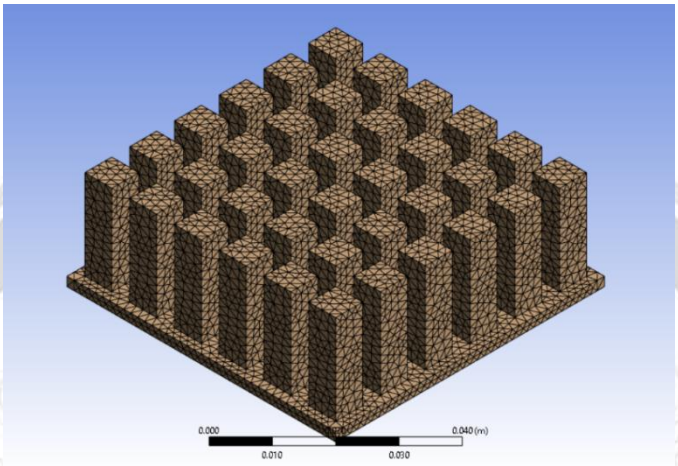

Fig.2: The mesh generated in the heat sink.

Table 1. Different grids and their T*w* different cases at Re=10000

case	Number of grid elements	T*w*
Fin spacing (2mm)	982352	321.70
	1194966	321.25
	1439210	321.4
	1733951	321.22
Fin spacing (4 mm)	882036	323.71
	1188661	322.56
	1422544	322.42
	1733010	322.54
Fin spacing (6mm)	1027747	323.72
	1183678	323.85
	1416080	.01324
	17321171	323.86
Height fin (20mm)	982352	321.70
	1194966	321.25
	1439210	321.4
	1733951	321.22
Height fin (27mm)	1042405	315.41
	1195570	315.08
	1442360	315.22
	1746673	315.078
Height fin (35mm)	1043467	310.53
	1198158	310.44

	1446949 1756069	310.24 310.11
A fin inclination of 5˚	1092387 1220023 1553428 1934205	309.96 309.82 309.74 309.8
A fin inclination of ˚15	1154210 1243580 1677288 1958824	307.74 307.52 307.60 307.53
A fin inclination of 25˚	1199520 1342100 1694210 1962425	308.38 308.09 308.16 308.01

The last row of the table was considered for each case.

4. Results and discussion

The obtained results of this section will be summarized according to the studied cases

4.1 validation

The obtained numerical model was validated through comparison with those of the reference study presented by Tariq et al [13]. In the current work, the computational domain considers air entering at a temperature of 23˚C, with an inlet velocity ranging from 2 to 8 m/s. The heat sink contains three fins with a constant heat flux of 8578 W/m². Each fins has a height 34 mm, a length of 34mm, and a thickness of 4mm, with a spacing of 6 mm between adjacent fins. Fig.2 illustrates the comparison between the present results and the reference data [15]. As can be seen, the agreement is acceptable, with only minor deviations, confirming the model's accuracy for further parametric studies.

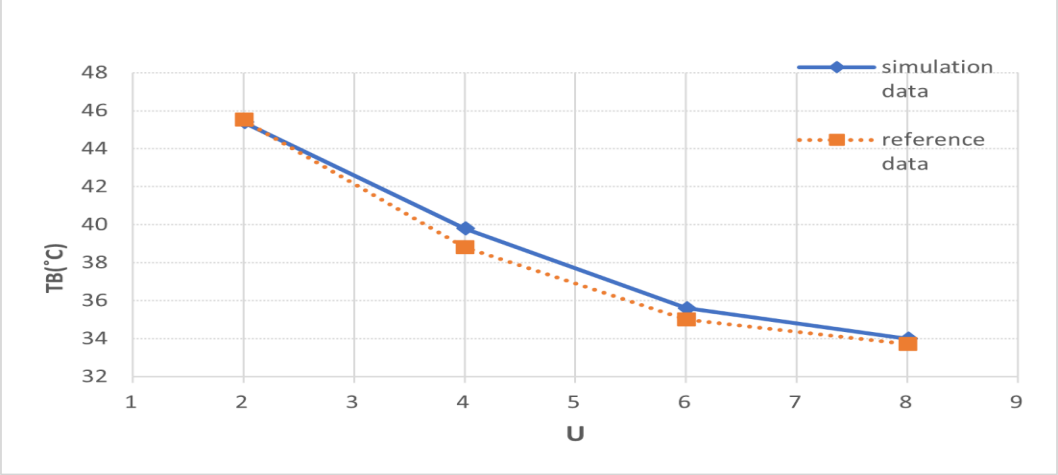

Fig.2: Comparison between the present and published results at[15]

Vol. 34, No. 1. \ 2026 ISSN: 2616 - 9916

4.2 Effect of spacing between fins

Fig.3 shows the relationship between bottom surface temperature (Tw) and Reynolds number (Re) for three different spacings (s1 2mm, s2 4mm, and s3 6mm). In general, the results showed a downward trend for (Tw) with the increase of Re in all cases, which reflects improvement in thermal performance as a result of the heat transfer rate. The lowest temperature was recorded at 2 mm for all Re. At 4mm, the values of temperature were slightly higher, and at 6mm, an increase in temperature was observed across all Reynolds number. This reflects a deterioration in thermal performance as a result of fin spacing and the decrease in thermal mixing effect. This indicates that reducing the spacing enhances cooling efficiency by increasing the effect of the generated turbulence with the near-wall fluid layer

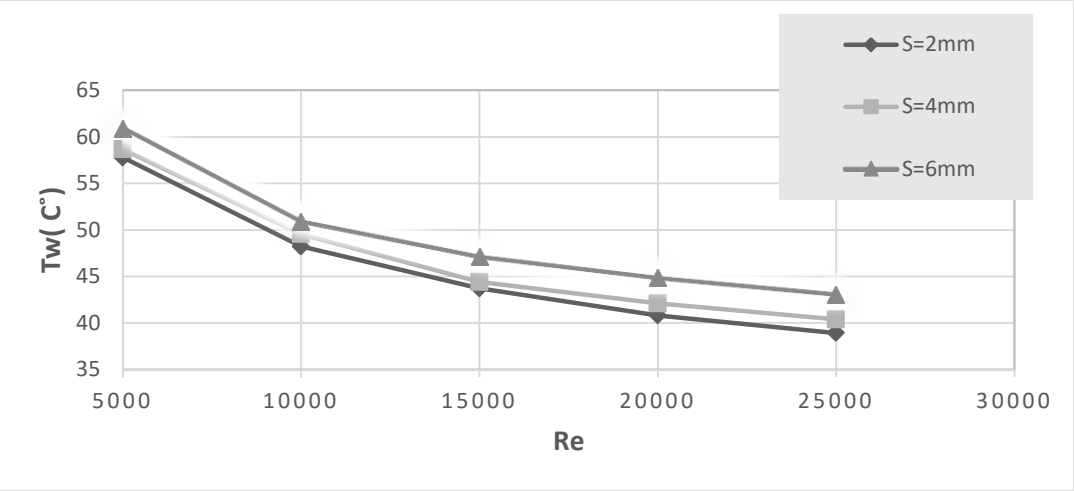

Fig.3: Effect of space between fins on the heated wall

Fig.4 illustrates the variation of the temperature difference between the heated wall temperature (T_w) and bulk air temperature (T_b) with Reynolds number (Re) for three different spacings between the fins (2mm, 4mm, and 6mm), a significant invrese relationship is recorded between Re and the temperature difference for all cases. At a lower Reynolds number (Re=5000), the temperature difference is higher for all spacings, with the largest spacings (s=6mm) resulting in ($\Delta T=32^{\circ}C$). The smallest spacing (s 2mm) repeatedly leads to the lowest (Tw-Tb) values across the Re range. This can be attributed to a higher surface area- to-volume ratio and increased thermal conduction paths that facilitate faster heat dissipation.

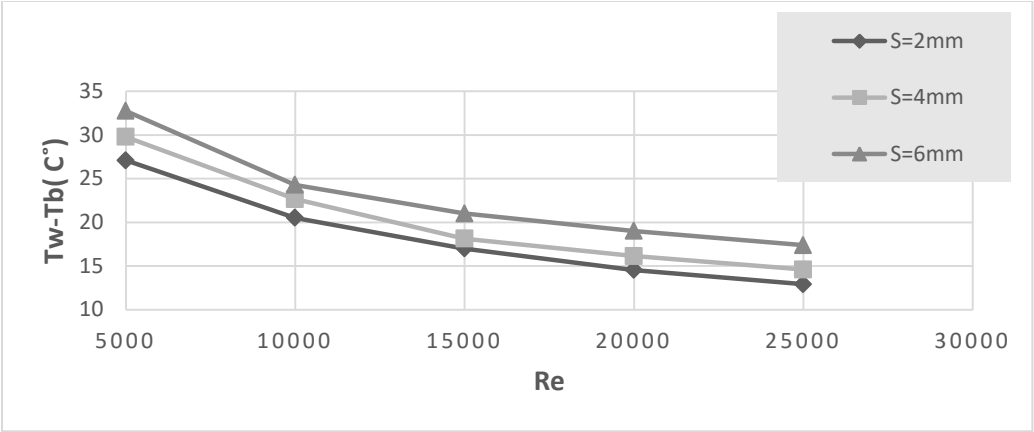

Fig.4: Effect of space between fins on the temperature difference($T_w - T_b$)

Fig.5 depicts the relationship between Reynolds number and Nusselt number for three spaces of fins (2mm, 4mm, and 6mm). The results showed an increase in Nusselt number with the increase of the Reynolds number. this indicates improved thermal performance due to an increase in velocity due to an increase in turbulence and enhanced thermal mixing in the channel. As shown in the figure, the least spacing (2mm) yields the highest Nusselt number along all Reynolds numbers, followed by the 4mm spacing, and then the 6mm spacing. At Re =25000, the highest Nusselt number is about 1100 for 2mm spacing, while it is approximately 950 and 820 for the 4mm and 6mm spacings.

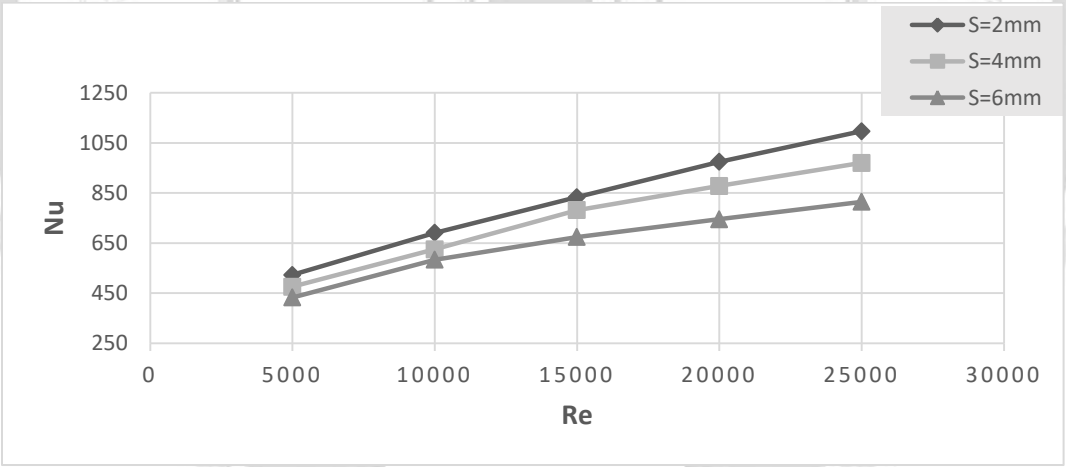

Fig.5: Impact of spaces between fins on the average Nusselt number.

4.3 Effect of height fins

Fig. 6 illustrates the variation in bottom surface temperature (T_w) with Reynolds number (Re) for three different fin heights (20 mm, 27 mm, and 35 mm). The findings clearly indicate an inverse relationship between Re and surface temperature (T_w) for all heights. The configuration with a height of 35 mm had the lowest (T_w) value among the cases studied. This signifies a

superior thermal performance at this height, presumably because of improved airflow penetration and more effective interaction between the heated surface and coolant. Conversely, the 20 mm height configuration resulted in the highest surface temperature at all Re, the configuration of 27 mm illustrated intermediate performance, with Tw value lower than those at 20 mm, but higher than at 35mm.

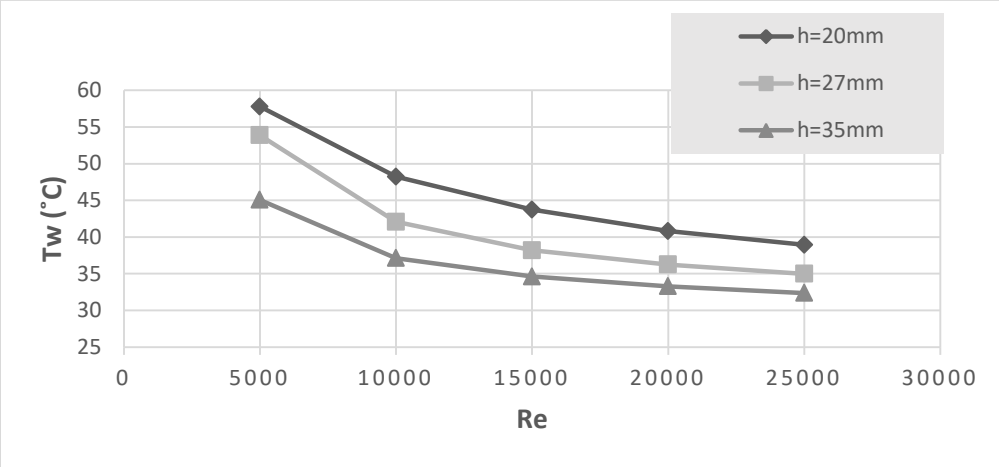

Fig.6: Effect of the height of the fin on heated wall temperature.

Fig.7 illustrates the alteration of temperature difference between the bottom wall of the heat sink (T_w) and bulk temperature (T_b) with Reynolds number (Re) for three different heights (20 mm, 27 mm, and 35 mm). As can be seen, increasing the Reynolds number constantly decreases the Tw-Tb difference across all cases. At lower Reynolds numbers, the temperature difference is considerably higher, especially for the smallest fin height (20 mm). The case with the tallest fins (35mm) showed the lowest temperature difference. The height of 27 mm shows intermediate behavior, consistently lying between the other two cases, demonstrating that a large heat transfer surface area enhances thermal performance. This response can be caused by improved mixing and raised flow disturbance near the heated surface, which decreases the thickness of the thermal boundary layer.

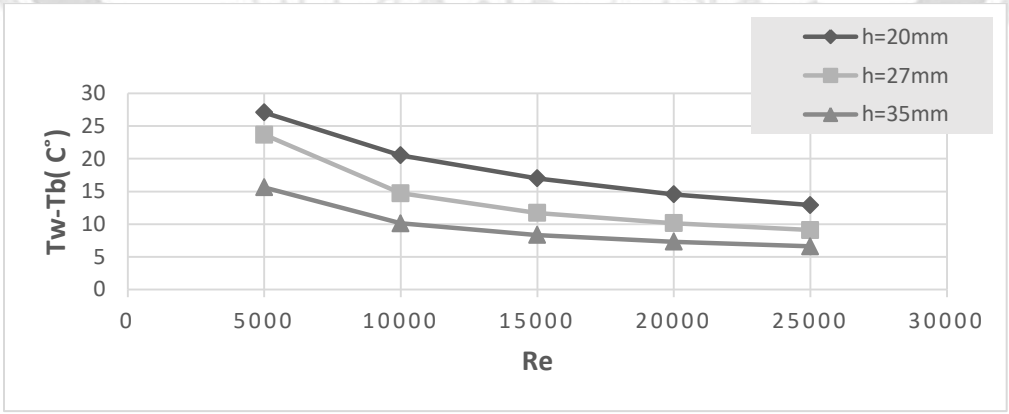

Fig. 7: Effect the height of the fin on temperature difference ($T_w - T_b$)

Fig. 8 illustrates the relationship between the Reynolds number (Re) and Nusselt number (Nu) for three different heights (20 mm, 27 mm, 35 mm), the data showed a clear positive correlation between Re and Nu throughout all heights, for h=35mm the Nu showed highest values compared with the other two cases, demonstrating that a large heat transfer surface area enhances thermal performance. This response can be caused by improved mixing and raised flow disturbance near the heated surface.

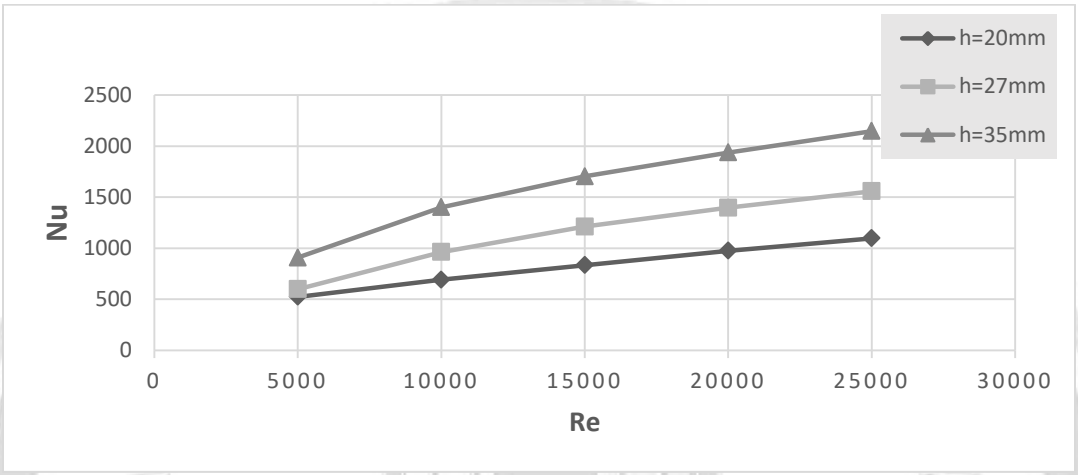

Fig.8: Effect of the height of the fin on the average Nusselt number.

4.4 Effect of angle

Fig. 9 illustrates the relationship between the Reynolds number (Re) and heated wall temperature (T_w) for square fins evaluated at three inclination angles (5°, 15°, and 25°) relative to the vertical axis, including the baseline case with an uninclined fin (α=0°). The observations reveal a consistent decrease in heated wall temperature (T_w) with increasing Re across all cases, indicating enhanced convective heat transfer due to increased flow turbulence. Fin angle has a considerable effect on thermal performance. Across the tested configurations, the 15° inclined fin consistently yields the lowest heated wall temperature over the entire range of Reynolds numbers. This indicates superior thermal enhancement, likely due to optimal vortex generation and enhanced fluid mixing, which in turn decreases the thermal boundary layer thickness. In comparison, the 25° inclined fin also demonstrates improved performance relative to the reference (α=0°).

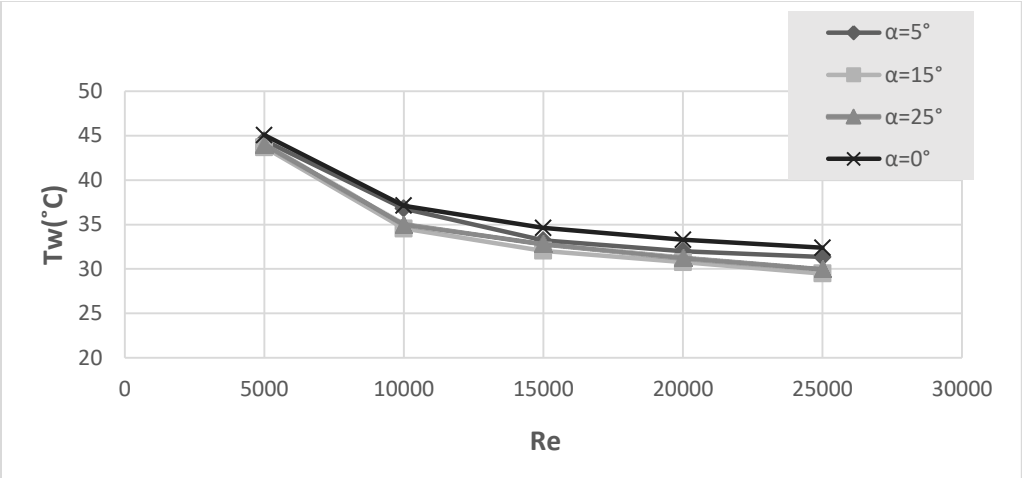

Fig.9: Effect of angles on heated wall temperature.

Fig.10 illustrates the variation of the temperature difference between the heated wall temperature and bulk temperature ($T_w - T_b$) across a range of Reynolds numbers (Re) for square vertical fins with three different inclination angles (5°, 15°, and 25°). Across all the evaluated cases, fins at 15° regularly attained the lowest ($T_w - T_b$) values across the Reynolds number range, which demonstrates their superior heat transfer capacity compared to the reference case (α=0°), fin inclined at 25° were slightly less effective than those 15°. Fins with 5° inclination demonstrated only slight improvement over the vertical case. The vertical fins (α=0°) showed the highest temperature difference, signifying the lowest thermal performance due to limited turbulence generation and weaker convective effects

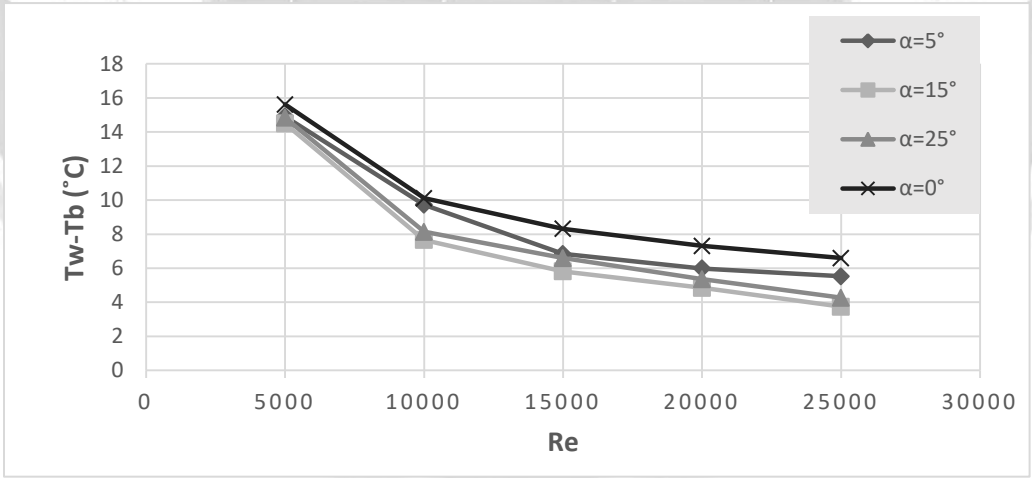

Fig.10: Effect of angles on temperature difference ($T_w - T_b$).

Fig.11 displays the relationship between the Reynolds number (Re) and Nusselt number (Nu) for various fin inclination angles (5°, 15°, and 25 °) of a square vertical fin and compares with the baseline. Nu progressively rises with the rise of the Re. Among the tested cases, the fins inclined 15° constantly achieve the highest Nu throughout the full range of Re. The improved thermal efficiency is ascribed to enhanced vortex generation and increased flow mixing, which strengthens the local convective heat transfer coefficient and decreases the thermal resistance. The fins with 25° inclination present a marginal performance compared to the 15° case. The 5° inclined fins display a moderate enhancement over the base case, while the vertical fins (α=0°) consistently yields the lowest Nusselt number.

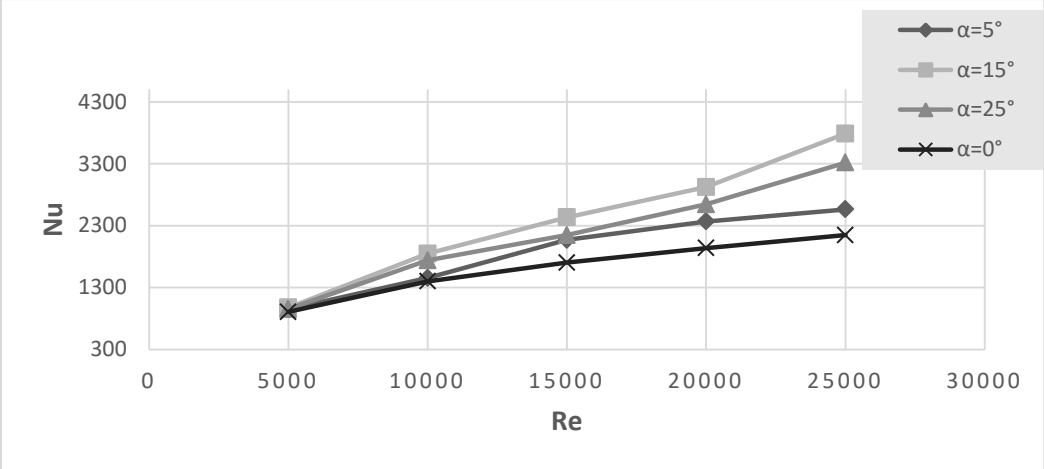

Fig.11: Effect of angles on average Nusselt number

Fig.12 displays the temperature contours of square fins with three different spaces between the fins: (a) the space between the fins is 2mm, (b) the space between the fins is 4mm, and (c) the space between the fins is 6mm. An obvious axial gradient noted from the inlet side (blue /green) toward the outlet (yellow, orange, red) reflecting the increase in base and fin temperature along the airflow path due to boundary layer growth and the reduction of the effective temperature difference, edge and corner fins appear slightly cooler than the interior rows caused by greater exposure to side flow and directional convective paths the fin tips are cooler than their bases with a vertical gradient within each fin. The results obtained from the temperature contours show that the case with a fin spacing of (2mm) attains the lowest surface temperature, followed by 4mm, while the (6mm) spacing displays the highest temperature. This behavior unveils that the smaller spacing leads to an increase in surface area for each fin.

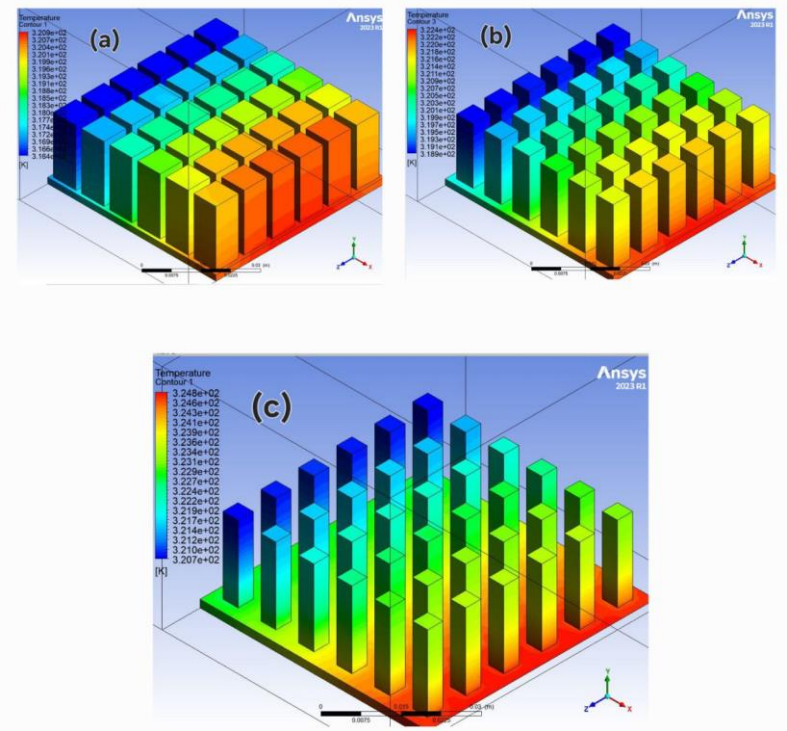

Fig.12: Temperature contours of three different distances: a) 2mm, b) 4mm, and c) 6mm.

Fig.13 shows the temperature contours of square fins with three different heights: (a) the height is 20mm, (b) the height is 27 mm, and(c) the height is 35mm. A clear improvement in thermal performance with increasing height, greater height (35mm) increases the surface area exposed to convection and extends the conduction path within the fin, lowering the base and average surface temperature. From the legends, the coldest case is the tallest, 35mm, the maximum temperature was 320.9 K, followed by the 27mm, the maximum temperature was 316.7 K, while the 20 mm showed the highest temperature (311.5K). Better temperature uniformity: larger height reduces the temperature difference between the rows (more uniform color distribution), which indicates more uniform heat distribution and lower risk of hot spots at the base. Boundary layer growth: As the air flows over the fin rows, the local heat transfer coefficient declines, which causes the heat transfer to be more efficient in the first rows than the last rows. This is evident in all heights, but in the case of 35 mm, due to the large surface area.

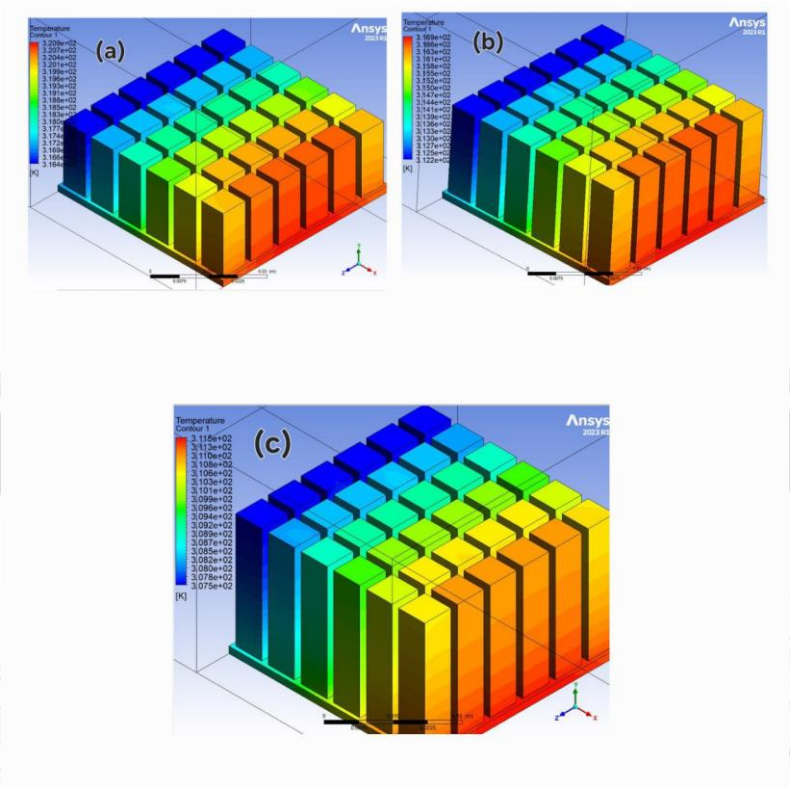

Fig.13: Temperature contours at three various fin heights: a) 20mm, b) 27mm, and c) 35mm.

Fig.14 presents the temperature distribution contour for square fins a heat sink in rectangular channel: (a) inclined fins with angle 5°, (b) inclined fins with angle 15°, and (c) inclined fins with angle 25°. As seen in figure the thermal distribution display fairly uniform pattern with distinct temperature gradient from the base (top) in the direction of the fin's tips. The moderate temperature gradient along the fin height demonstrating effective mixed heat transfer by conduction within the fin and on the external surface by convection with a raised inclination angle to 25°, a small change of the color gradient between the fins is recorded, with a slightly greater decrease in the higher temperature at the base compared to case (a). And at 15°, the effect became clearer: a greater decline in peak temperatures seems to occur, along with color waves pointing to greater cooling variation through the rows.

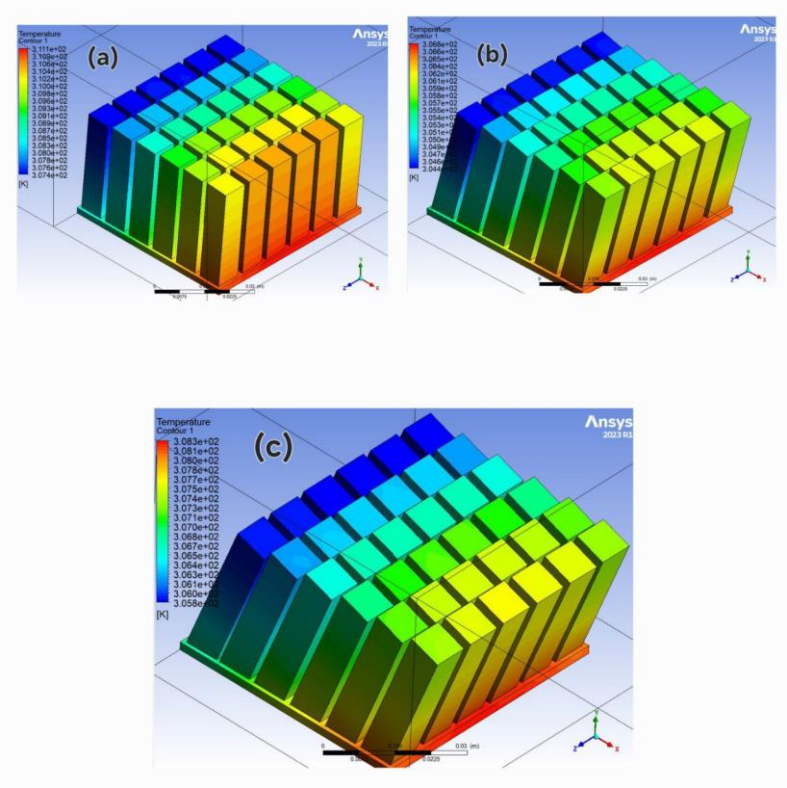

Fig.12: Temperature contours of three different angles: a) 5˚, b) 15˚, and c) 25˚.

10. Conclusion

The investigation reported here numerically analyzed the thermal performance of a heat sink positioned in a rectangular channel, concentrating on the effect of the fin spacing, fin height, and fin inclination angle. The main results are summarized as follows:

1. Reducing fin spacing improves cooling performance. At Re = 25,000, decreasing spacing from 6 mm to 2 mm reduced wall temperature by 9% and increased the Nusselt number by 41%. Smaller improvements were observed between 4 mm and 2 mm (5%, 16%), while moderate enhancement occurred between 6 mm and 4 mm (5%, 22%). Overall, the smallest spacing (2 mm) showed the best thermal performance.
2. Increasing the fin height from 20 mm to 35 mm reduced the heated surface temperature from 38.9˚C to 32.37˚C (16% reduction) and enhanced the Nusselt number from 1096 to 2147.2 (94% increase).
3. Increasing the fin angle from 5˚ to 15˚ reduced the surface temperature by about 6% and enhanced the Nusselt number by 48%.

References

[1] Sun, Peiqi, Mohd Azmi Ismail, and Ahmad Fikri Mustaffa. "Metamodel-based design optimization for heat transfer enhancement of finned heat sinks." International Journal of Thermal Sciences 214 (2025): 109896.

[2] Mushatet, Khudheyer S., and H. M. Hmood. "Numerical investigation for heat transfer enhancement in a triangular twisted tube." *ARPN Journal of Engineering and Applied Sciences* 16.5 (2021): 593-599.

[3] Y. Huang, S. Shen, H. Li, and Y. Gu, "Improved thermal design of fin heat sink for high-power LED lamp cooling," *2016 17th Int. Conf. Electron. Packag. Technol. ICEPT 2016*, no. August 2016, pp. 1069–1074, 2016, doi: 10.1109/ICEPT.2016.7583311.

[4] H. M. Jaffal, "The Effect of Fin Design on Thermal Performance of Heat Sink," *J. Eng.*, vol. 23, no. 5, pp. 123–146, 2017, doi: 10.31026/j.eng.2017.05.09.

[5] K. S. Mushatet and N. M. Bader, "Thermal Performance Assessment for The Solar Air Collector Integrated with Ribs Turbulators under Nassiriya City Climate," vol. 45, no. 2, pp. 166–174, 2022.

[6] H. Sivasankaran, G. Asirvatham, J. Bose, and B. Albert, "Experimental analysis of parallel plate and crosscut pin fin heat sinks for electronic cooling applications," *Therm. Sci.*, vol. 14, no. 1, pp. 147–156, 2010, doi: 10.2298/TSCI1001147S.

[7] A. A. A. Jabber, M. R. Jawad, A. Abdul, and M. Humadi, "the Effect of Heat Sink Fins Length and Material on Its Performance," no. December, 2016.

[8] S. B. Chin, J. J. Foo, Y. L. Lai, and T. K. K. Yong, "Forced convective heat transfer enhancement with perforated pin fins," *Heat Mass Transf. und Stoffuebertragung*, vol. 49, no. 10, pp. 1447–1458, 2013, doi: 10.1007/s00231-013-1186-z.

[9] T. Science, "Numerical Study Of Laminar Flow In A Sudden Expansion Obstacled Channel," Vol. 19, No. 2, Pp. 657–668, 2015, Doi: 10.2298/Tsci121029105m.

[10] R. Sam Sukumar, Sb. Arun, Pd. kumar, C. Naidu, A. Professor, and B.-T. student, "Modelling And Analysis Of Heat Sink With Rectangular Fins Having Through Holes," *Ch.Sanyasi Naidu / Int. J. Eng. Res. Appl.*, vol. 3, no. April 2013, pp. 1557–1561, 2013, [Online]. Available: www.ijera.com

[11] K. A. M. Annuar and F. S. Ismail, "Optimal pin fin arrangement of heat sink design and thermal analysis for central processing unit," *2014 5th Int. Conf. Intell. Adv. Syst. Technol. Converg. Sustain. Futur. ICIAS 2014 - Proc.*, no. February, 2014, doi: 10.1109/ICIAS.2014.6869537.

[12] M. Hatem, H. Abdellatif, and W. Hussein, "Enhancement of Perforated Pin-Fins Heat Sink under Forced Convection," *Int. Res. J. Eng. Technol.*, no. October, 2020, [Online]. Available: www.irjet.net

[13] Nashee, Sarah, and Khudheyer S. Mushatet. "Performance study on turbulent heat transfer using rectangular air duct integrated with continuous and intermittent ribs turbulators." *Thermal Science* 00 (2024): 214-214. https://doi.org/10.2298/TSCI240430214N

[14] A. Saif Al Kindi and A. AL Kindi, "Experimental and Numerical Analysis of Air Flow Through Heat Sink Fins," *Proc. ISER Int. Conf.*, no. November, pp. 1–5, 2020, [Online]. Available: https://www.researchgate.net/publication/346396925

[15] A. Tariq, K. Altaf, S. W. Ahmad, G. Hussain, and T. A. H. Ratlamwala, "Comparative numerical and experimental analysis of thermal and hydraulic performance of improved plate fin heat sinks," *Appl. Therm. Eng.*, vol. 182, p. 115949, 2021.

[16] M. A. H. Abdelmohimen, S. Algarni, K. Almutairi, G. M. S. Ahmed, K. Irshad, and S. A. Irfan, "Improving Heat Transfer of Plate-Fin Heat Sinks Using through Rod Configurations," *J. Therm. Sci. Eng. Appl.*, vol. 13, no. 1, 2021, doi: 10.1115/1.4046984.

[17] A. A. Mohammed and S. A. Razuqi, "Performance Of Rectangular Pin-Fin Heat Sink Subject To An Impinging Air Flow," *J. Therm. Eng.*, vol. 7, no. 3, pp. 666–676, 2021, doi: 10.18186/THERMAL.889174.

[18] P. İ. M. Kanatçikli, I. S. I. Kuyulari, and İ. Deneysel, "2nd INTERNATIONAL BAKU CONFERENCE ON SCIENTIFIC RESEARCH April 28-30, 2021 / Baku, AZERBAIJAN," pp. 34–48, 2021.

[19] R. B. Gurav, P. Purohit, and S. P. Nalavade, "Computational Study on Forced Convection Heat Transfer in Pin Fin Heat Sink (PFHS) with Inclined Wings," *J. Phys. Conf. Ser.*, vol. 2601, 2023, doi: 10.1088/1742-6596/2601/1/012026.

[20] R. A. Al-Luhaibi and I. T. Nazzal, "Investigation of Heat Sinks with Different Perforation Patterns," *Int. J. Heat Technol.*, vol. 41, no. 5, pp. 1195–1204, 2023, doi: 10.18280/ijht.410510.

[21] K. S. Mushatet and R. A. Fayyad, "Experimental Investigation For Performance Evaluation Of Solar Air Heater Collector," *AIP Conf. Proc.*, vol. 2398, no. October, 2022, doi: 10.1063/5.0093799.

[22] B. Çiçek, "Numerical investigation on thermal behaviors of Heat Sinks and Hybrid Heat Sinks with different PCMs for electronic cooling," *Adv. Mech. Eng.*, vol. 16, no. 8, pp. 1–17, 2024, doi: 10.1177/16878132241269229.

[23] Nashee, Sarah Rabeea, and Khudheyer Salim Mushatet. "Impact of Ribs with Multiple Arrangements on the Behavior of a Turbulent Flow in a Rectangular Channel." *Journal of Heat and Mass Transfer Research* 12.2 (2025): 259-270. 10.22075/jhmtr.2025.34713.1575.

[24] M. S. Sukri and V. V. Wanatasanappan, "Numerical Analysis on Heat Sinks with Different Geometries for PC Cooling System," *AIP Conf. Proc.*, vol. 2799, no. 1, 2024, doi: 10.1063/5.0181996.

[25] A. Azirul, A. Ibrahim, N. S. Nazri, H. Jarimi, M. A. A. Mohd Zainuri, and U. Syafiq, "PVTE system performance improvement via numerical optimization of heat sink design and fluid working conditions," *Sci. Rep.*, vol. 15, no. 1, pp. 1–16, 2025, doi: 10.1038/s41598-025-97461-x.

[26] I. T. Nazzal, T. K. Salem, and R. R. J. Al Doury, "Theoretical Investigation of a Pin Fin Heat Sink Performance for Electronic Cooling using Different Alloys Materials," *IOP Conf. Ser. Mater. Sci. Eng.*, vol. 1094, no. 1, p. 012087, 2021, doi: 10.1088/1757-899x/1094/1/012087.

[27] Mushatet, Khudheyer S. "Simulation of laminar natural convection in a cavity with cylindrical obstacles." *Australian Journal of Basic and Applied Sciences* 5.6 (2011): 636-645.

[28] Razzaq, Ali K. Abdul, and Khudheyer S. Mushatet. "A numerical study for a double twisted tube heat exchanger." Journal homepage: http://iieta. org/journals/ijht 39.5 (2021): 1583-1589. https://doi.org/10.18280/ijht.390521.

[29] Nashee, Sarah Rabeea, Zainalabden A. Ibrahim, and Dhuha J. Kamil. "Numerical investigation of flow in vertical rectangular channels equipped with three different obstacle shapes." *AIP Conference Proceedings*. Vol. 3122. No. 1. AIP Publishing LLC, 2024. https://doi.org/10.1063/5.0216016

[30] M. Hatem, H. Abdellatif, and W. Hussein, "Enhancement of perforated pin-fins heat sink under forced convection," International Research Journal of Engineering and Technology (IRJET), vol. 7, no. 10, pp. 1440–1446, Oct. 2020.

[31]A. A. Mohammed and S. A. Razuqi, "Performance of rectangular pin-fin heat sink subject to an impinging air flow," Journal of Thermal Engineering, vol. 7, no. 3, pp. 666–676, Mar. 2021.

ARTICLE
JOURNAL`S UNIVERSITY OF BABYLON FOR ENGINEERING SCIENCES (JUBES)
مـــجلـة جـــامعة بـــابـل للعلـــوم الهندسية
Vol. 34, No. 1. \ 2026 ISSN: 2616 - 9916

دراسة عددية لمبدد حرارة ذي زعانف مربعة بزوايا ميل مختلفة

فاطمة راسم خضير سالم مشتت

قسم هندسة الميكانيكية، كلية الهندسة، جامعة ذي قار 64001، العراق

fatima.r.n@utq.edu.iq

الخلاصة

تقدم هذه الدراسة بحثًا رقميًا لمبدد حرارة ذي زعانف في تدفق حراري قسري. أجريت الاختبارات على زعنفة مربعة بزوايا ميل وارتفاعات ومسافات متفاوتة بين الزعانف. تم فحص هذه المعلمات عند أرقام رينولدز مختلفة ضمن النطاق المضطرب (من 5000 إلى 25000) وتدفق حراري قدره 5000 واط/م². تم نمذجة توزيع الحرارة وسلوك التدفق حول المبدد الحراري باستخدام معادلات نافييه–ستوكس الكاملة ومعادلات الطاقة. تم إجراء المحاكاة باستخدام ANSYS Fluent مع نموذج k–ε. أشارت النتائج إلى أن تقليل المسافة بين الزعانف من 6 مم إلى 2 مم أدى إلى انخفاض بنسبة 9٪ في درجة حرارة السطح وزيادة في رقم نسلت بنسبة 41٪، مما يسلط الضوء على تحسن كبير في نقل الحرارة بالحمل الحراري. وبالمثل، أظهرت التغيرات في ارتفاع الزعانف تأثيرًا ملحوظًا على السلوك الحراري، مما أدى إلى انخفاض بنسبة 16٪ في درجة حرارة السطح وزيادة رقم نسلت بنسبة 94٪، وتبين أن الميل 15 يوفر الأداء الحراري الأمثل بين الزوايا التي تم فحصها، حيث حقق أدنى درجة حرارة سطح بنسبة 6٪.

الكلمات الدالة:– مشتت حراري، زعانف مربعة، أداء حراري.